University College London

Final year project

Optical Ptychographic Phase Tomography

Author:

Qiaoen Luo

Supervisors:

Prof. Ian Robinson

Dr. Fucai Zhang

March 20, 2013

Abstract

The possibility of combining ptychographic iterative phase retrieval and computerised tomography using optical waves was investigated in this report. The theoretical background and historic developments of ptychographic phase retrieval was reviewed in the first part of the report. A simple review of the principles behind computerised tomography was given with 2D and 3D simulations in the following chapters.

The sample used in the experiment is a glass tube with its outer wall glued with glass microspheres. The tube has a diameter of approximately 1 mm and the microspheres have a diameter of 30 μm. The experiment demonstrated the successful recovery of features of the sample with limited resolution. The results could be improved in future attempts. In addition, phase unwrapping techniques were compared and evaluated in the report.

This technique could retrieve the three dimensional refractive index distribution of an optical component (ideally a cylindrical object) such as an opitcal fibre. As it is relatively an inexpensive and readily available set-up compared to X-ray phase tomography, the technique can have a promising future for application at large scale.

Contents

List of Figures **i**

1 Introduction **1**

2 Theory **3**

2.1 Phase Retrieval 3

2.1.1 Phase Problem 3

2.1.2 The Importance of Phase 5

2.1.3 Phase Retrieval Iterative Algorithms 7

2.2 Ptychography 9

2.2.1 Ptychography Principle 9

2.2.2 Ptychographic Iterative Engine 11

2.2.3 Other Ptychographic Iterative Algorithms 15

2.2.4 New Developements 15

2.3 Tomography 16

2.3.1 Introduction 16

2.3.2 Radon Transformation 16

2.3.3 Backprojection 18

2.3.4 Fourier Slice Theorem 18
2.3.5 Reconstruction Approach 19
2.4 Phase tomography 20

3 Experiments **22**
3.1 Ptychography 22
3.1.1 Fresnel Diffraction 22
3.1.2 Experiment Set-up and Alignment 22
3.1.3 2D Image 25
3.1.4 Projection of a 3D Structure 26
3.2 Phase tomography 29
3.2.1 Simple Simulations 29
3.2.2 Computing Approach 31
3.2.3 3D Reconstruction 33
3.2.4 Evaluation 37

4 Conclusion **42**

Bibliography **50**

Appendix A List of Main Equipments **51**

List of Figures

2.1 A random phase change will alter the image more than a random magnitude change. 6

2.2 A schematic for single iteration in a typical phase retrieval algorithm [Bean, 2012] 9

2.3 A schematic for PIE algorithm demonstrating the scanning of four diffraction pattern [Rodenburg and Faulkner, 2004] 12

2.4 The coordination system for the Radon transform 17

3.1 Setup of the experiment including keyparts such as the light source, the pinhole, the motor stages, the sample, and the detector. 23

3.2 Close-up of the sample and the stage system which consists of three translation stages and one rotation stages. . 24

3.3 2D image of a microscopy slide glued with glass beads with size of 30μm. 25

3.4 Reconstructed image of a 2D scan of the 3D tube sample. 26

3.5 Zoom-in in another reconstructed image of a 2D scan of the 3D tube sample. 27
3.6 Sample projection demonstrating the reduced quality of data used for tomographic reconstruction. 28
3.7 The original image, its sinogram and reconstructed (unfiltered and filtered) images of a “Shepp-Logan” phantom 29
3.8 Simulation of the reconstruction of 3D object using proposed computing approach. 30
3.9 Wrapped phase of a projection. 32
3.10 Phase map of projections from computing the derivative of unwrapped regions at two different angles. Fig. 3.10(a) and Fig. 3.9 are of the same area for the same projection. 32
3.11 Generation of sinograms and filter backprojection of each sinogram to generate its respective slice in the tomogram. 33
3.12 Slices of the reconstructed tomogram 35
3.13 Projection at 90 degree. 36
3.14 Central slice of tomogram cutting at the middle of the projection in Fig. 3.13 36
3.15 Conventional Goldstein unwrapping 38
3.16 Computation of derivation 39

Chapter 1

Introduction

The increasing demand for high resolution imaging in research areas such as biology and material science has rendered conventional lens imaging techniques impractical. The resolution of these imaging techniques are restricted by the quality and the resolving power of the lens used. The cost of manufacturing the lenses of high quality with large numerical aperture (NA) is prohibitive. More importantly, the system is fundamentally diffraction limited [Born and Wolf, 1999] so that resolution in the order of nano meter is difficult to achieve.

Several schemes were devised to break the limits involving the use of fluoroscent dyes and total internal reflection of light source [Zhuang, 2009; Huang et al., 2008; Schermelleh et al., 2010]. Coherent Diffractive Imaging (CDI) offers another solution. Phase retrieval from the light diffracted by the object gets rid of the restriction placed on the spatial resolution by removing the lens from the imaging system. Through advanced iterative algorithms, the phase introduced by the object can

be now retrieved to form images with resolution around 10 nano meters using X-ray [Thibault et al., 2008].

Tomography, on the other hand, has been a well-established technique to reconstruct three dimensional object from its two dimensional projections. It is thus to our interest to perform tomography using the projections obtained through phase retrieval techniques (CDI and Ptychographic CDI). This synthesis of techniques was already demonstrated on a range of samples using the X-ray [Dierolf et al., 2010a; Trtik et al., 2012; Esmaeili et al., 2013; Guizar-Sicairos et al., 2011; Holler et al., 2012; Lima et al., 2012].

This experiment aims to test the methods using optical waves, investigate the problems encountered and discuss the possible application. This technique is particularly useful in imaging three-dimensional distribution of refractive indices of a sample (a cylindrical object ideally) that has a high optical wave transmissivity, such as an optical fibre. In fact, the two-dimensional optical phase imaging has already proven to be commercially successful in revealing the quality of contact lenses [Maiden et al., 2012b].

Chapter 2

Theory

2.1 Phase Retrieval

2.1.1 Phase Problem

In the typical set-up for CDI, the diffraction patterns are collected in far-field Fraunhofer diffraction regime where the diffracted wave $F(\mathbf{u})$ is the fourier transform of the density distribution of the object $f(\mathbf{x})$. [Born and Wolf, 1999] as indicated by:

$$\mathcal{F}[f(\mathbf{x})] = \int f(\mathbf{x}) e^{i2\pi(\mathbf{ux})} d\mathbf{x} = F(\mathbf{u}) \tag{2.1}$$

$$\mathcal{F}^{-1}[F(\mathbf{u})] = \int F(\mathbf{u}) e^{-i2\pi(\mathbf{ux})} d\mathbf{u} = f(\mathbf{x}) \tag{2.2}$$

where Eq. 2.1 and Eq. 2.2 are Fourier transformation and inverse Fourier transformation and $\mathbf{x}$ are real space coordinate and $\mathbf{u}$ are reciprocal space coordinate with $\mathbf{x} = (x_1, x_2, x_3)$ and $\mathbf{u} = (u_1, u_2, u_3)$. The

$d\mathbf{x}$ and $d\mathbf{u}$ terms represent volume elements.

To compute such Fourier transformations with data collected from the detector, Fast Fourier Transform (FFT) [Seiler and Seiler, 1989] is a powerful function that can be employed to solve discrete Fourier transforms as follows:

$$F(u) = \sum_{x=0}^{N-1} f(x) exp(-i2\pi u * x/N) \tag{2.3}$$

$$f(x) = N^{-2} \sum_{u=0}^{N-1} F(u) exp(i2\pi u * x/N) \tag{2.4}$$

As the diffracted wave $F(\mathbf{u})$ is complex valued, it can be written in terms of magnitude and phase as follows:

$$F(\mathbf{u}) = |F(\mathbf{u})| exp[i\psi(\mathbf{u})] \tag{2.5}$$

where ψ represents phase.

The detector can only pick up the intensity of the signals. The intensity is related to $|F(\mathbf{u})|^2$ but not to the phase. The inverse Fourier transformation of the intenstiy provides the autocorrelation $f(\mathbf{-x}) * f(\mathbf{x})$ of the object. The phase problem is thus to find the sample image fuction, $f(\mathbf{x})$, from the intensity. The missing part of $f(\mathbf{x})$ is its exponetial term which represents the phase information.

2.1.2 The Importance of Phase

In conventional imaging in which lenses are used, the lenses can perform inverse Fourier transform to retrieve $f(\mathbf{x})$ from $F(\mathbf{u})$ without the lost of the phase information. In diffractive lenseless imaging, the inverse Fourier transform step will be computed instead.

In reality, the missing half of the information: the phase information is much more important than the magnitude part. To understand the reason behind it, Parseval's theorem must be first introduced.

Mathematically, in context of discrete Fourier transforms, Parseval's Theorem can be manifested as:

$$\sum_{x=0}^{N-1} |f(\mathbf{x})|^2 = \frac{1}{N} \sum_{u=0}^{N-1} |F(\mathbf{u})|^2 \tag{2.6}$$

A trivial result of Parseval's Theorem stated above is that the theorem can be interpreted as follows:

Parseval's Theorem. *The mean-square value on one side of the Fourier transform is proportional to the mean-square value on the other side of the Fourier transform.*

So that:

$$rms(f(\mathbf{x})) \propto rms(F(\mathbf{u})) \tag{2.7}$$

As Fourier transform is additive, the following equation is also valid:

$$rms(\Delta f(\mathbf{x})) \propto rms(\Delta F(\mathbf{u})) \tag{2.8}$$

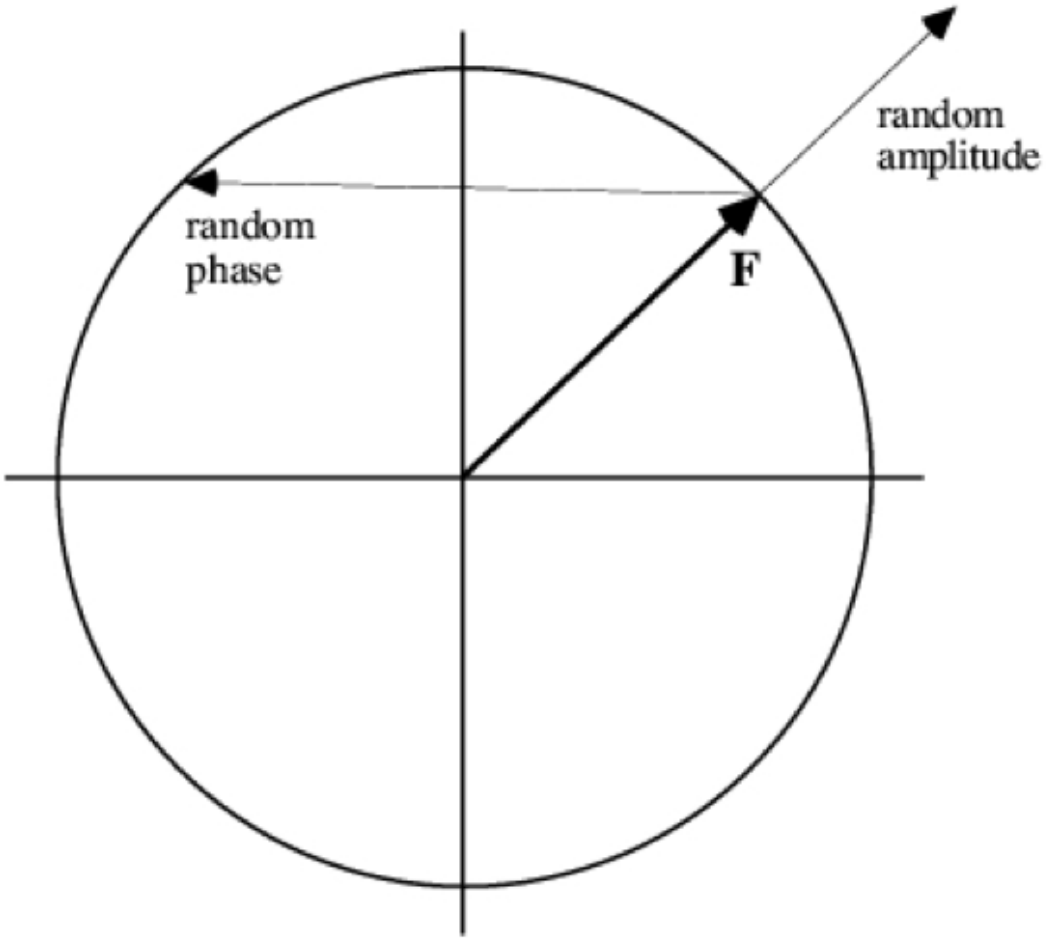

Figure 2.1: A random phase change will alter the image more than a random magnitude change.

A smaller root mean error in the image in the real space would be introduced by a change in the magnitude in the frequency domain. On the contrary, a much bigger root mean error in real space would be introduced by the same amount of change in the phase in the frequency domain as shown in Fig. 2.1.

Unless a priori information is assumed, the phase information in Fourier domain contributes more in defining the structure of the image in real space. As a priori information is often not readily available, it

is worth invesitigating how to obtain phase from the data collected by the detector. Hence, phase problem is an important research area in imaging science.

2.1.3 Phase Retrieval Iterative Algorithms

In CDI, the diffraction pattern provides an equation that can be solved to retrieve the phase which, by offsetting, represents the phase change induced by the sample in the illumination wave function in real space. With a priori information (for example, the periodicity of a unit cell in a crystal), this set of equations can be solved more easily to image the object (the crystal). This technique was widely used in Crystallography to determine the structure of crystalline material.

Based on Shannon sampling theorem [Shannon, 1949], Miao and Sayre suggested that even an aperiodic object in real space can be reconstructed if enough diffractions of the object in reciprocal space are collected [Miao et al., 1999; Sayre, 1952].

A series of developments in iterrative algorithms was developed since 1972. Essentially similiar in principle with the "oversampling" approach, these algorithms provides support and constraints to fascilitates the convergence of solving the set of equations to obtain a phase distribution. Gerchberg and Saxton [Gerchberg and Saxton, 1972] first came up with a working iterative algorithm capable of solving phase problem. Later, Fienup, based on their algorithm, devised the Error Reduction (ER) and the Hybrid Input-Output (HIO) algorithms [Fienup, 1978, 1982,

1987]. He later employed methods to tackle the stagnation problems [Fienup and Wackerman, 1986] thus enhancing the performance of each algorithm. In a typical CDI experiment, a combination of ER and HIO algorithms is used.

All of the aforementioned algorithms work by first providing an initial guess about the object in real space, then discretely Foureir transforming the guess to reciprocal space by using the FFT function mentioned earlier. By updating the transformed wave function with the magnitude derived from the intensity data collected, the magnitude-corrected function is then inverse discrete Fourier transformed back to real space. Real space constraints such as non-negativity or other a priori information are then applied to the function to generate a new guess in the real space domain. By repeating the steps, the algorithm can approach a set of answers for the set of equations through a number of iterations given that the calculation converges. A flow chart demonstrating the process in one iteration is as shwon in Fig. 2.2 provided by [Bean, 2012].

The algorithms differ in their approaches mostly on how to update the guess in the real space. The nature of the specific sample imaged in the experiment is an important factor for selecting the appropriate algorithm. A more comprehensive comparison of various algorithms on their principle and performance could be found in [Marchesini, 2007; Yang et al., 2011]. Mathematicians offered mathematical insights as they perceived phase retreival algorithms as an numerical optimisation

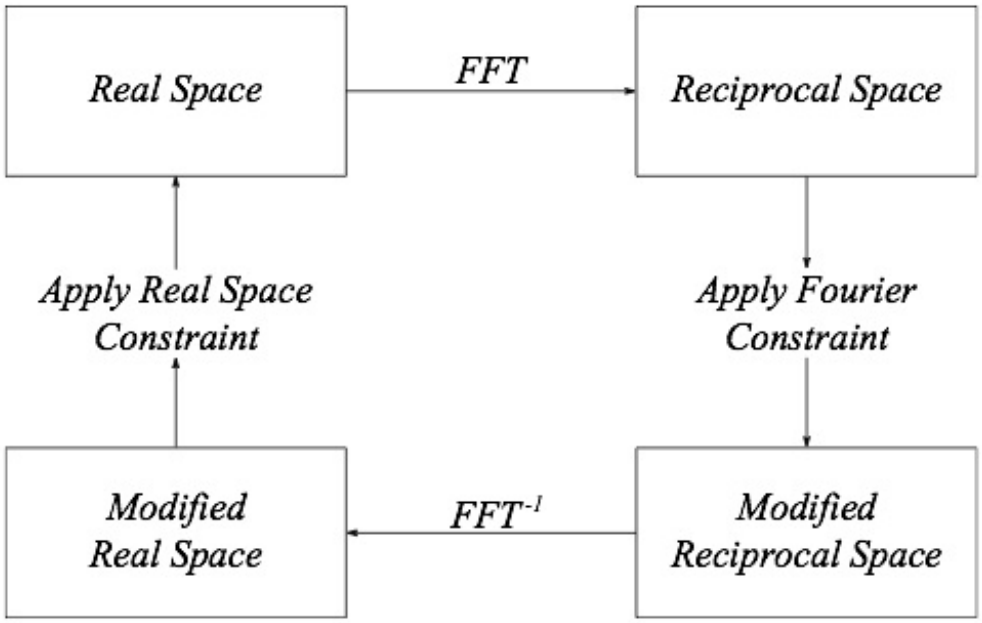

Figure 2.2: A schematic for single iteration in a typical phase retrieval algorithm [Bean, 2012]

problem [Dong et al., 1996; Bauschke et al., 2002; Yang et al., 2011].

2.2 Ptychography

2.2.1 Ptychography Principle

Ptychography was first conceived and described by Hoppe in 1968-1973 [Hegerl and Hoppe, 1970]. Hoppe overlapped adjacent Bragg reflections to interfer them coherently by placing a narrow aperture in the object plane in order to solve phase problem with the information given by the redundancy in measurements. In the overlapped region, the sum of intensities provide more information on what the phases of $F(\mathbf{u})$ can be. Due to the limited hardware quality and technology in the 70s,

the idea was only demonstrated by imaging a crystalline object using a scanning transmission electron microscope. A good demonstration of the principle using atomic scaled wavelength was not given until [Nellist et al., 1995].

The nature of ptychography is as the Greek word "Ptycho" suggested, the folding of diffractions via the convolution of the Fourier transform of an illumination function in the object plane [Rodenburg, 2008].

It is assumed that for a thin (2D) object, the exit wave is the multiplication of the illumination function and the object function.

If the exit wave from the object is defined as:

$$\psi_f(\mathbf{x}) = p(\mathbf{x}) * o(\mathbf{x}) \tag{2.9}$$

where $p(\mathbf{x})$ and $o(\mathbf{x})$ are the illumination function and the object function respectively.

The convolution theorem at Fraunhofer plane gives the Fourier transformed $\psi_f(x, y)$ to be:

$$\psi_F(\mathbf{u}) = \{\mathcal{F}[p(\mathbf{x})]\} \oplus \{\mathcal{F}[o(\mathbf{x})]\} \tag{2.10}$$

Or:

$$\psi_F(\mathbf{u}) = P(\mathbf{u}) \oplus O(\mathbf{u}) \tag{2.11}$$

where $P(\mathbf{u})$ and $O(\mathbf{u})$ are the Fourier transformed $p(\mathbf{x})$ and $o(\mathbf{x})$ and

the convolution operator $\oplus$ is defined as:

$$P(\mathbf{u}) \oplus O(\mathbf{u}) = \int\int P(\mathbf{u}) * O(\mathbf{u\text{-}U}) d\mathbf{U} \tag{2.12}$$

where $\mathbf{U}$ is of the same nature as $\mathbf{u}$ as convolution represents the integral of the product of the two functions after one is reversed and shifted.

The ptychography problem is to deconvolute Eq. 2.11 and solve for $p(\mathbf{x})$ and $o(\mathbf{x})$ in real space from the intensity measured by the detector.

In 1992, Rodenburg and Bates suggested that ptychography problem can be solved by a method called "Wigner Deconvolution" [Rodenburg and Bates, 1992]. However, it was proven that solving through Wigner Deconvolution was not a realistic practice as the probe translation was required to be smaller than the resolution of the reconstructed image [Yang et al., 2011].

2.2.2 Ptychographic Iterative Engine

In 2004, Rodenburg and Faulkner suggested a phase retrieval algorithm which used ptychographic principle decoupling the object, $o(\mathbf{x})$, and probe, $p(\mathbf{x})$, (or the illumination function) [Rodenburg and Faulkner, 2004]. This algorithm, later named as "Ptychographic Iterative Engine (PIE)", has proved to be robust and stable. As diffraction patterns can be scanned across a bigger surface in this ptychographic, the field of view was enlarged. The schematic for the algorithm is shown in Fig. 2.3.

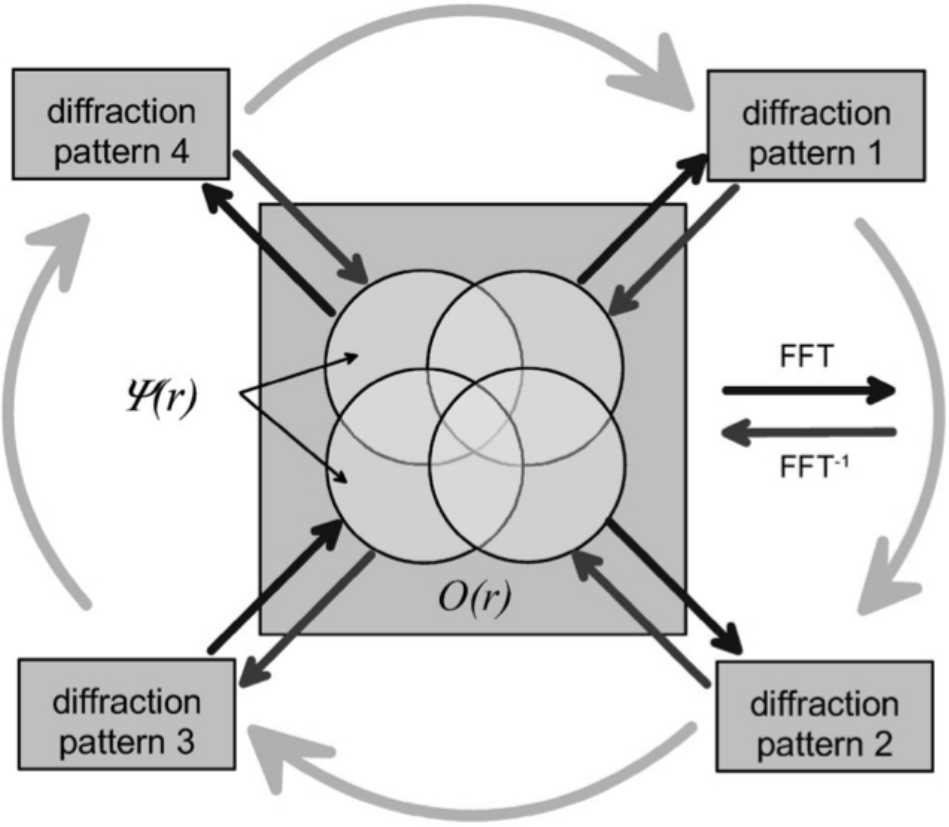

Figure 2.3: A schematic for PIE algorithm demonstrating the scanning of four diffraction pattern [Rodenburg and Faulkner, 2004]

The PIE algorithms works with the following steps [Rodenburg and Faulkner, 2004]:

1. The object function is guessed to be $o_{g,n}(\mathbf{x})$, where g indicates it is a guessed solution while n denotes it is the guess in the nth iteration.

2. The exit wave is the multiplication of $o_{g,n}(\mathbf{x})$ and $p(\mathbf{x}\text{-}\mathbf{R})$ which indicates the current guesss at the current position at $\mathbf{R}$:

$$\psi_{g,n}(\mathbf{x},\mathbf{R}) = o_{g,n}(\mathbf{x})p(\mathbf{x}\text{-}\mathbf{R}) \tag{2.13}$$

3. $\psi_{g,n}(\mathbf{x},\mathbf{R})$ is then Fourier transformed to be $\Psi_{g,n}(\mathbf{u},\mathbf{R})$ whose magnitude is then replaced by the real magnitude $|\Psi(\mathbf{u},\mathbf{R})|$ to form the new exit wave function $\Psi_{c,n}(\mathbf{u},\mathbf{R})$:

$$\psi_{c,n}(\mathbf{u},\mathbf{R}) = |\psi(\mathbf{u},\mathbf{R})| exp(i\theta_{g,n}(\mathbf{u},\mathbf{R})) \tag{2.14}$$

where $\theta_{g,n}$ is the phase.

The new exit wave function is then inverse Fourier transformed to an improved version of the exit wave $\psi_{c,n}(\mathbf{x},\mathbf{R})$.

4. Then the guessed object is updated by the "update function", $U(\mathbf{x})$:

$$O_{c,n+1}(\mathbf{x}) = O_{c,n}(\mathbf{x}) + U(\mathbf{x}) * \beta(\psi_{c,n}(\mathbf{x},\mathbf{R}) - \psi_{g,n}(\mathbf{x}-\mathbf{R})) \tag{2.15}$$

where the $U(\mathbf{x})$ is given by:

$$U(\mathbf{x}) = \frac{|P(\mathbf{x}-\mathbf{R})|}{|P_{max}(\mathbf{x}-\mathbf{R})|} \frac{P^*(\mathbf{x}-\mathbf{R})}{|P(\mathbf{x}-\mathbf{R})|^2 + \alpha} \tag{2.16}$$

where α is a constant to prevent the case when the denominator is zero and β is a feedback parameter varied between aproximately 0.5 and 1.

This ptychographic phase retrieval algorithm had room for improvements. The major experimental difficulty is to know the accurate information about the probe. Nonetheless, this reinvented ptychographic approach on phase retreival opened up a lot of opportunities in research

areas such as X-ray, optical imaging and electron microscopy as it offers a wide field of view with resolution beyond the diffraction limit.

In 2008, Maiden and Rodenburg improved PIE algorithm by including the update function for the probe [Maiden and Rodenburg, 2009]. The extended ptychographic iterative algorithm (ePIE) [Maiden and Rodenburg, 2009] is not restricted by the prior knowledge of the probe. The update functions are as follows:

$$O_{c,n+1}(\mathbf{x}) = O_{c,n} + \frac{P^*_{c,n}(\mathbf{x}-\mathbf{R})}{|P_{c,n}(\mathbf{x}-\mathbf{R})|^2_{max}} * \beta(\psi_{u,n}(\mathbf{x},\mathbf{R}) - \psi_{c,n}(\mathbf{x},\mathbf{R})) \tag{2.17}$$

$$P_{c,n+1}(\mathbf{x}) = P_{c,n} + \frac{O^*_{c,n}(\mathbf{x}-\mathbf{R})}{|O_{c,n}(\mathbf{x}-\mathbf{R})|^2_{max}} * \alpha(\psi_{u,n}(\mathbf{x},\mathbf{R}) - \psi_{c,n}(\mathbf{x},\mathbf{R})) \tag{2.18}$$

The probe and object wavefronts are both retrieved using the improved algorithm. As a result, in theory, any shape of the probe can be used, even a probe that is modulated by a diffuser can be used. Compared to other algorithms which will be mentioned in the later chapter, the ePIE algorithm has proven to be very robust to noise and it also demonstrated speedy convergence in the simulations [Maiden and Rodenburg, 2009].

2.2.3 Other Ptychographic Iterative Algorithms

There are also other phase retrieval algorithms which utilise the ptychographic concept of scanning overlapping regions of the sample to reconstruct the object wavefront.

One algorithm, the "difference map" is developed by Elser in 2003 [Elser, 2003]. The algorithm, then tested by Thibault in a scanning x-ray diffraction microscope in 2008 [Thibault et al., 2008], has become the major algorithm for X-ray ptychography in Swiss Light Source.

Guizar and Fienup also provided another algorithm named "non-linear optimization" method [Guizar-Sicairos and Fienup, 2008]. There is another approach in which Fresnel CDI and ptychography is combined [Vine et al., 2009]. The details of these algorithms are not explained explicitly here because ePIE algorithm adapted for near-field Fresnel diffraction was used in the experiment to obtain the set of projections used for the tomographic reconstruction.

2.2.4 New Developements

Other than X-ray ptychography, optical ptychography has shown promising imaging potential. Quantitative phase images of healthy and cancerous cells were imaged using optical ptychography [Claus et al., 2012].

As ptychography presents a wide ranged application prospect, many scientists have dedicated efforts in improving the existing algorithms. The ePIE was improved in terms of resolution by a factor of 3 by incorporating a phase ramp into each iteration of algorithm [Maiden et al.,

2011]. Several scientists have suggested position correction algorithms [Maiden et al., 2012a] to further enhance the performance of ePIE.

2.3 Tomography

2.3.1 Introduction

Tomography is a non-destructive imaging technique that can reveal the inner features of an object by providing 2D sections at different depths or angles. Computerised Tomography (CT) has been used in the medical field for radiological diagnostics since the 70s.

Modern tomography involves more powerful and sophisticated reconstruction algorithms using signal acquisition media not limited to X-ray. Other physical phenomenon used includes gamma rays, radio-frequency waves, electrons and so on. In this experiment, optical waves were used and a developed reconstruction approach called filtered backprojection (FBP) was used to reconstruct 3D images from 2D projections.

2.3.2 Radon Transformation

Radon transformation is the underlining mathematical principle in tomography. It describes the relationship between the density of an object and its scattering projections.

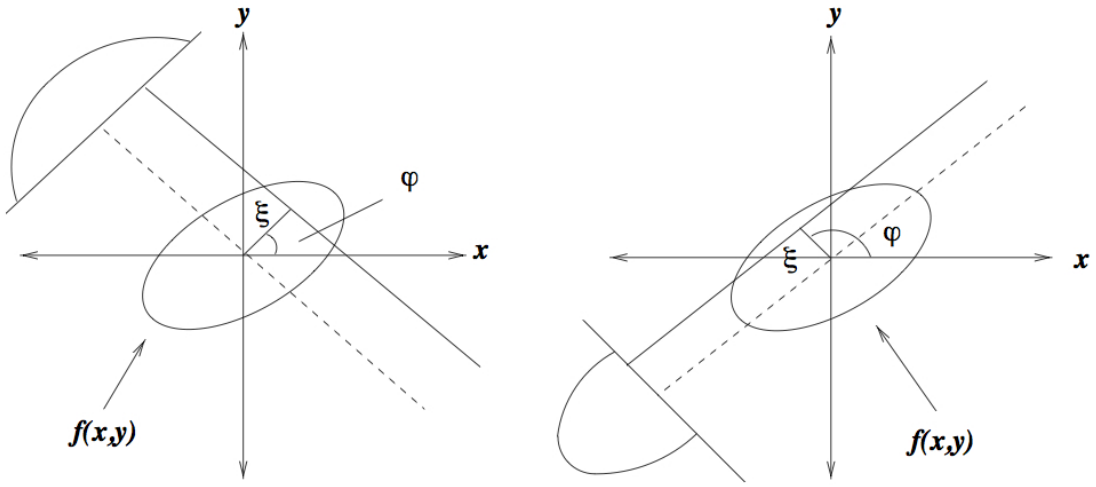

Figure 2.4: The coordination system for the Radon transform

As Fig. 2.4 has shown, a 2D Radon transformation can be writtern as:

$$\rho(\xi, \psi) = \int f(x, y)\delta(xcos\psi + ysin\psi - \xi)dxdy \tag{2.19}$$

where the $\rho(\xi, \psi)$ is the output of the transform, known as a sinogram and $f(x, y)$ represents the density of the object.

In a physical example, the scattering X-ray is collected with varying attenuation based on the different density of the object. Hence, an inverse radon transformation can regenerate a distribution of density where X-ray scanned. However, it is difficult to just apply the mathematically defined inverse radon transformation in a numericallly fast and computationally economical way. Hence, other reconstruction approaches were suggested to compute the 3D structure of an object.

2.3.3 Backprojection

Backprojection is an applicable approach to carry out reconstruction. It is defined as an integral of sinograms over all angles, an equivalent of propagating the sinogram back to the image space along the projection path. Backprojection can be written as:

$$f_{BP}(x,y) = \int_0^{\pi} \rho(xcos\psi + ysin\psi, \psi)d\psi \tag{2.20}$$

As a simulation result in Chapter 3.2.1 has indicated, a backprojection produces blurry images. A simple ramp of $\frac{1}{|R|}$ in the real space can be applied to remove the blur. Filtered backprojection in real space is thus defined as:

$$f_{FBP}(x,y) = \frac{1}{|R|} \oplus f_{BP} \tag{2.21}$$

where $\oplus$ is the convolution relationship described by Eq. 2.11. It is noted that different kinds of ramps can be applied to relevant situations for different kinds of sample objects.

2.3.4 Fourier Slice Theorem

Given a set of projections at different angles, the task is to utilise FFT to quickly compute the reconstruction applying a ramp filter along the process. In order to achieve that, one has to use Fourier Slice Theroem.

According to [Kak and Slaney, 1988] in their renowned book "Principles of Computerised Tomographic Imaging", with adapted notations,

Fourier Slice Theorem is defined as:

Fourier Slice Theorem. *The Fourier transform of a parallel projection of an image $f(x, y)$ taken at angle ψ gives a slice of the two-dimensional transform, $F(u, v)$, subtending an angle ψ with the u-axis. In other words, the Fourier transform of $\rho(\xi, \psi)$ gives the values of $F(u, v)$ along the line ξ lies in Fig. 2.4.*

2.3.5 Reconstruction Approach

It is clear that, adapting the notations shown above, the steps for a reconstruction of a 2D image are as follows [Penczek, 2010]:

1. Compute a 1D Fourier transform of each projection of the image.
2. Multiply the Fourier transform of the projection with the ramp function deemed appropriate for the sample.
3. Inverse Fourier transform back the filtered projection.
4. Apply backprojection using Eq. 2.20 to complete the reconstruction of the 2D image.

To put the above steps to mathematical formulae, it can be shown as:

$$
\begin{aligned}
f(\mathbf{r}) &= \int_0^{\pi}\int_{-\infty}^{\infty} \mathcal{F}[\rho(r_\psi)] exp(-2\pi i \mathbf{r}\tau|\xi|) d\xi d\psi \\
&= \int_0^{\pi} \mathcal{F}^{-1}[|R| * \mathcal{F}[\rho(r_\psi))]] d\psi \\
&= Backprojection[Filtration(\rho)] \qquad (2.22)
\end{aligned}
$$

where the ramp filter is chosen as $|R|$ in the frequency domain.

There are many sophisticated reconstruction schemes for 3D reconstruction of an object, however, 3D reconstruction can be done by interpolating a stack of axial 2D reconstructions [Penczek, 2010] in order to save computational workload.

In this experiment, a reconstruction approach similiar to the aforementioned steps was used. By stacking the slices with appropriate interpolating technique, 3D structure of the sample was revealed.

2.4 Phase tomography

The concept of phase tomography was first suggested by Hoppe [Hoppe, 1982]. 2D Phase projections of a 3D structured sample can be processed using the aforementioned tomographic reconstruction procedures.

There are currently a few advanced techniques for 3D imaging. Rooted from fluoroscence microscopy, Zhuang invented stochastic optical reconstruction microscopy (STORM) [Zhuang, 2009] and applied to three dimensions achieving resolution as low as 20nm [Huang et al., 2008]. Serial

block-face scanning electron microscopy (SBFSEM) is another technique that provide 3D structural features in a scale of sub nanometers [Denk and Horstmann, 2004]. Recently, Bo Chen used both SBFSEM and ptychographic X-ray tomography to analyse the structure and percolation properties of marine coating [Chen et al., 2013]. Laminography is an imaging technology with the set-up very similiar with tomography: the detector and the sample both rotate in laminography circumventing the need to rotate angles more than 60 degrees [Kroupa and Jakubek, 2011]. A comparison of image quality between laminography and tomography can be found in [Xu et al., 2012].

X-ray phase tomography via CDI or ptychographic CDI have been successfully demonstrated on a variety of samples producing 3D images of high resolution. In 2010, Jiang conducted tomography of biological samples which are too thick for electron micrsocopy using projections from CDI at nanometer-scale [Jiang et al., 2010]. Using "difference map" algorithm, X-ray phase tomography via ptychography were demonstrated [Guizar-Sicairos et al., 2011; Dierolf et al., 2010a]. It was then applied to a wide-ranged variety of samples [Esmaeili et al., 2013; Dierolf et al., 2010b; Lima et al., 2012]. Instrumentation of the X-ray ptychographic phase tomography has already taken place [Holler et al., 2012].

Similiar 3D imaging has not been demonstrated using optical waves. This experiment intends to demonstrate this possibility.

Chapter 3

Experiments

3.1 Ptychography

3.1.1 Fresnel Diffraction

Unlike collecting data of Fraunhofer diffractions at the far-field in conventional CDI and X-ray Ptychography do, the detector, placed close to the sample, collects data of Fresnel diffractions in this experiment. By doing so, a large field of view can be achieved. It also saved space so that the experiment set-up can be compact.

3.1.2 Experiment Set-up and Alignment

The experiment set-up is as shown in Fig. 3.1. The set-up consists of three main parts: the sCMOS camera as the detector, the motor stage assembly and the light source. A more comprehensive list of equipments can be found in Appendix A. The stage assembly includes the translation

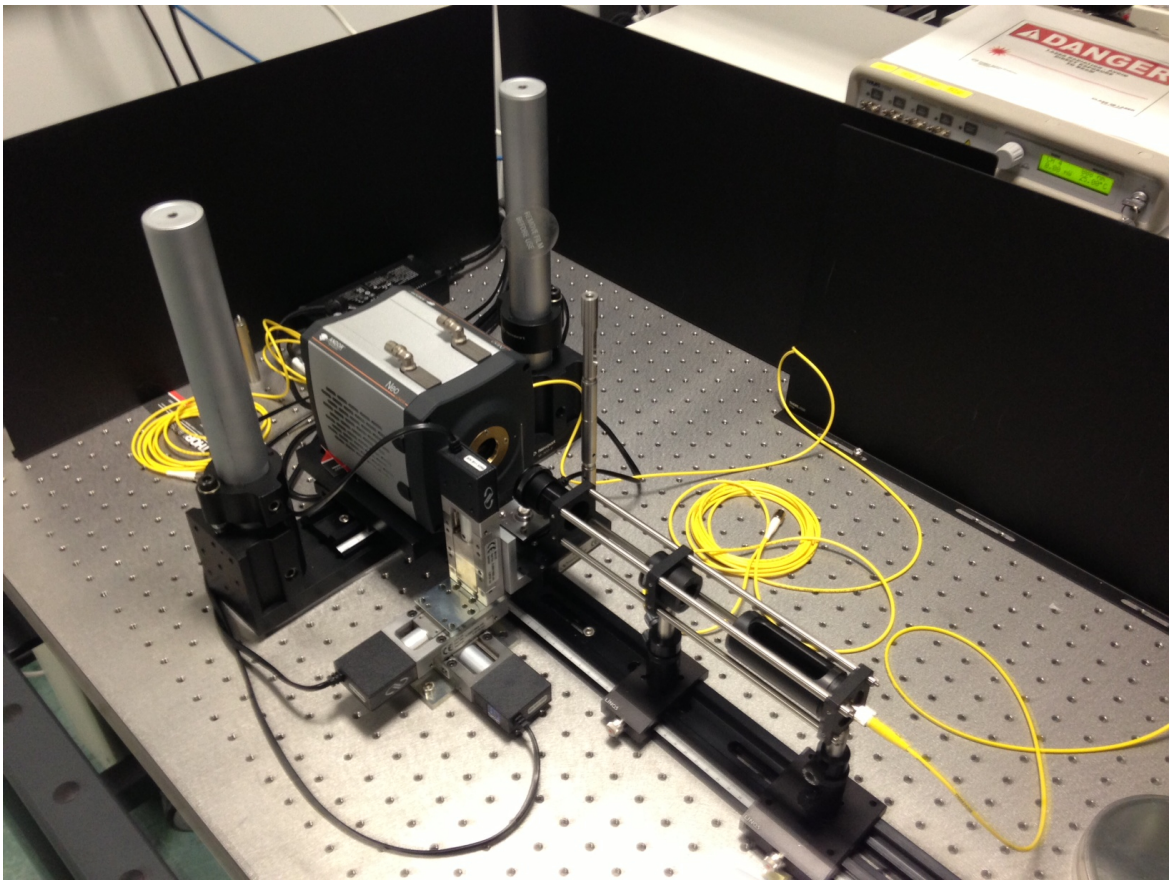

Figure 3.1: Setup of the experiment including keyparts such as the light source, the pinhole, the motor stages, the sample, and the detector.

stages which allow the ptychographic acquisition of fresnel diffraction patterns, a rotation stage which varies the angle of the sample with respect to the detector. The light source is a low-power green laser with wavelength of 543.5nm. The laser rays was first collimated by an aspheric lens and then modulated by a pinhole of size about 800nm. The pinhole is placed very near to the sample, less than 10mm. The pinhole size and wavelength of the light source are two crucial parameters for the recording and reconstruction. The pinhole-to-sample distance could be estimated at first in trial runs and refined for later collecting the whole set of diffractions.

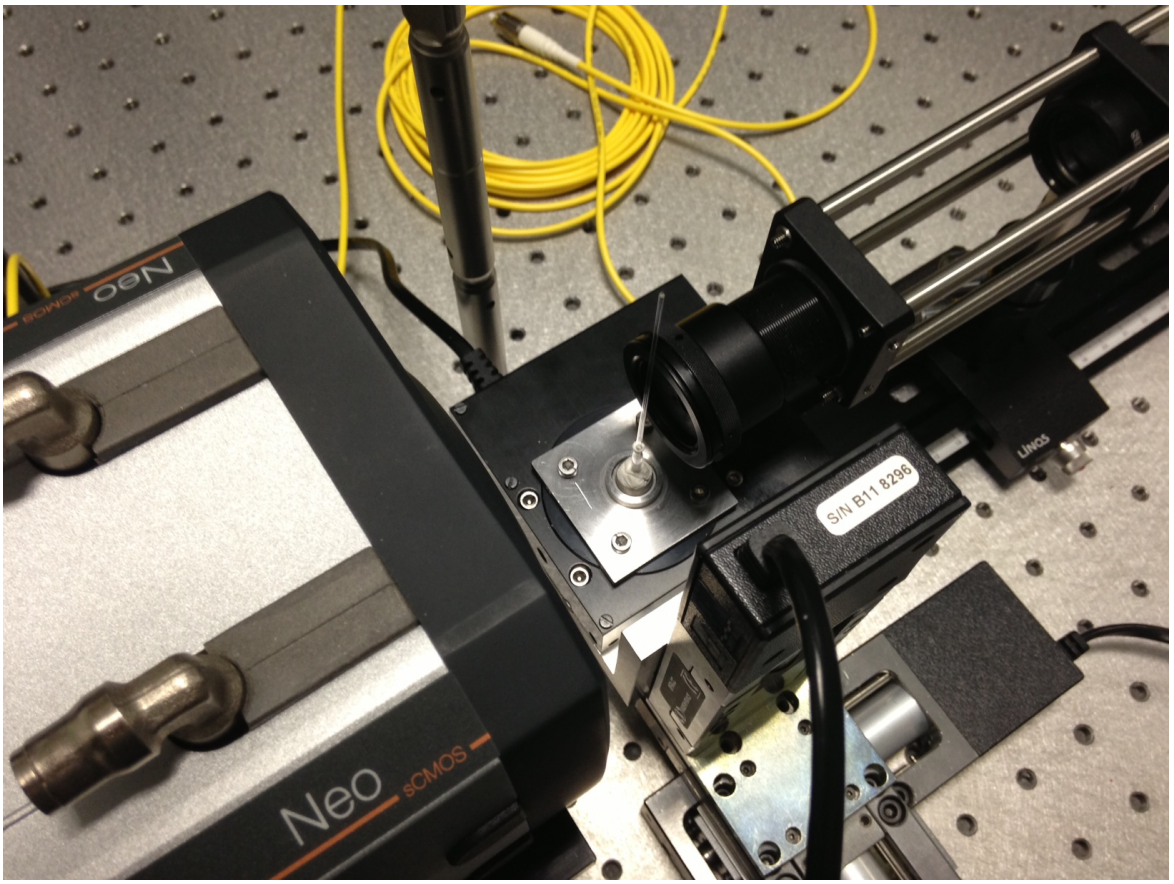

Figure 3.2: Close-up of the sample and the stage system which consists of three translation stages and one rotation stages.

A close-up on the relative positions of the stage assembly, the sample and the pinhole can be found in Fig. 3.2. The correct alignment of the stages is essential in guaranteeing the quality of both the reconstructed projections and the reconstructed 3D images. Not only the plane of the stages must be aligned, the plane of the motion of each plane has to be checked as well. Using the sCMOS, the alignment was checked and corrected to satisfactory levels.

3.1.3 2D Image

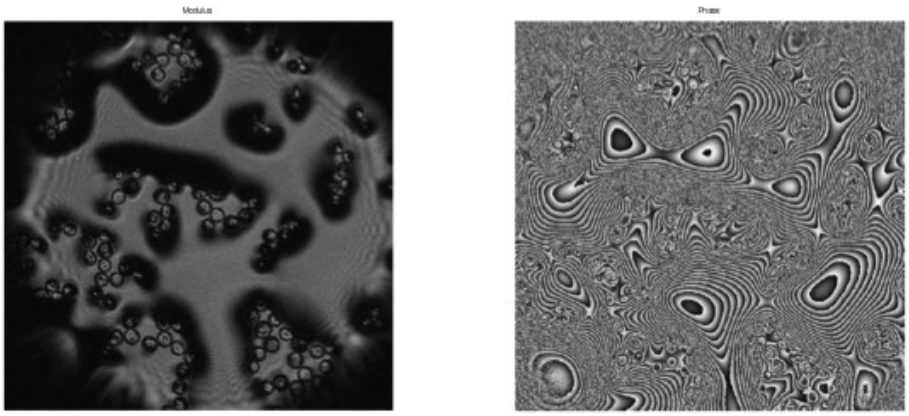

Figure 3.3: 2D image of a microscopy slide glued with glass beads with size of 30μm.

In this experiment, glass microspheres of size 30μm were deemed a suitable subject of interest. This was because they are transparent, they introduce phase changes if light encounters them and they are of the right size for optical ptychographic imaging. It was expected that the phase change introduced by these microspheres could be found at the end of this experiment. To verify that the microsheres were viable candidates for making the 3D sample, a ptychographic scan of a 2D slide glued with clusters of the microspheres was carried out. The resulted image is as shown in Fig. 3.3.

The locations of the microspheres were clearly revealed in both the magnitude and phase images. The black areas were likely due to the

uneven spread of the glue, so that the light rays got scattered out of the reception area of the detector. Hence, the microspheres were thought to be ideal for making 3D objects used in later stages of the experiment.

3.1.4 Projection of a 3D Structure

The 3D sample was made out of a glass tube of a diameter around 1mm. The glass tube was fixed by envoloping the pin of the sample holder. It was then cleaned thoroughly. Paper dipped in the glue was brushed over some glass microspheres. Then the paper was applied on the surface of the glass tube so that microspheres are attached on the tube.

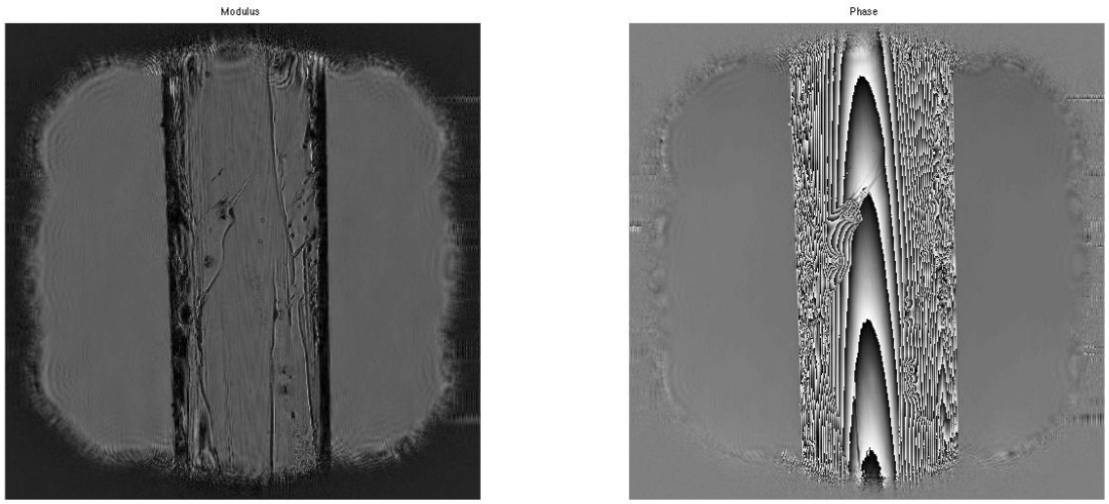

Figure 3.4: Reconstructed image of a 2D scan of the 3D tube sample.

Ptychographic phase retrieval was designed to image 2D object as the object has a well-defined position along the optical axis. Thus by imaging a 3D object using ptychographic phase retrieval, an ambiguity of the location of the object was introduced compromising the quality

of the image. This ambiguity is one of the systematic errors in the experiment.

Fig. 3.4 was obtained through 800 iterations of ePIE with position correction function (created by Dr. Fucai Zhang) turned on. This many-iteration result is of fine quality revealing the key features of the sample including the clear image of the glass microspheres, the glue distribution and the shape of the tube.

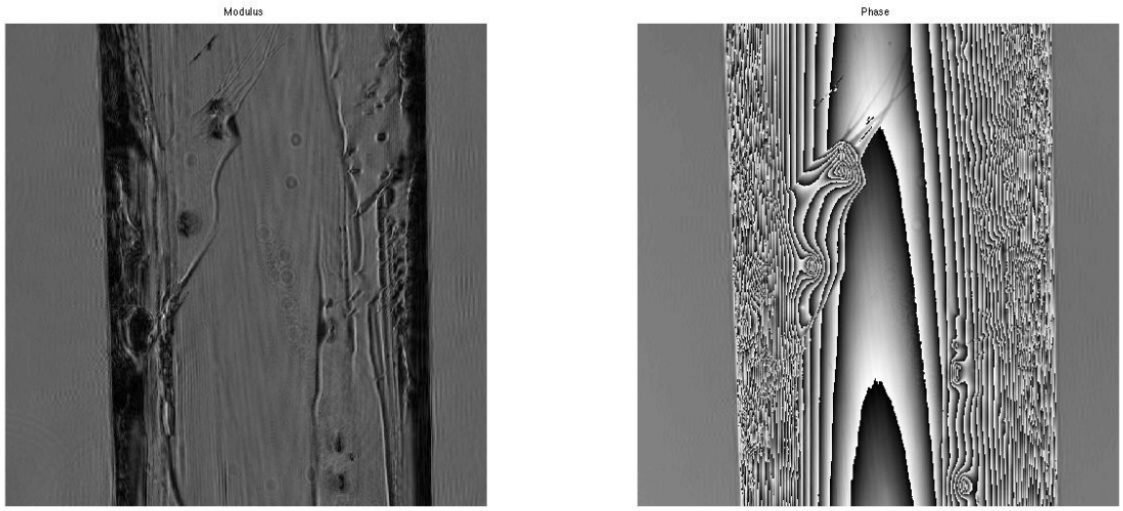

Figure 3.5: Zoom-in in another reconstructed image of a 2D scan of the 3D tube sample.

A closer look at another projection can be found in Fig. 3.5. It was noted then that the edges of the tube appear black in the magnitude map. The key question is that whether or not, the lost information on the edges can be recovered through computerised tomography.

In order to carry out tomographic reconstruction with a reasonable computational workload, each projection had to be compressed in size. A binning of detector pixels of "2×2" was used affecting the quality of

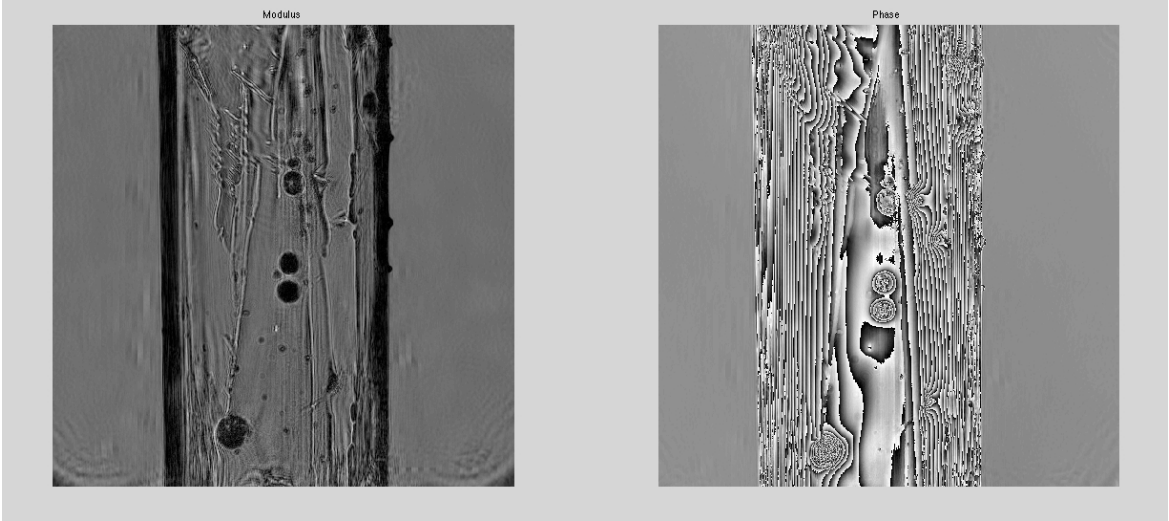

Figure 3.6: Sample projection demonstrating the reduced quality of data used for tomographic reconstruction.

the image as four pixels are effective one pixel in this binning setting. However, the computational workload is still quite sizable, and the whole acquisition and reconstruction time spent was long. The recording of 181 projections spanning from 0° to 180° took more than 12 hours while reconstruction of these 181 projections took more than that. A sample projection of such quality is shown in Fig. 3.6.

In the ptychographic reconstruction step, the reconstruction of each projection was then fed to the next projection to achieve better quality as a number of iterations were saved before the algorithm converged to correct solutions.

3.2 Phase tomography

3.2.1 Simple Simulations

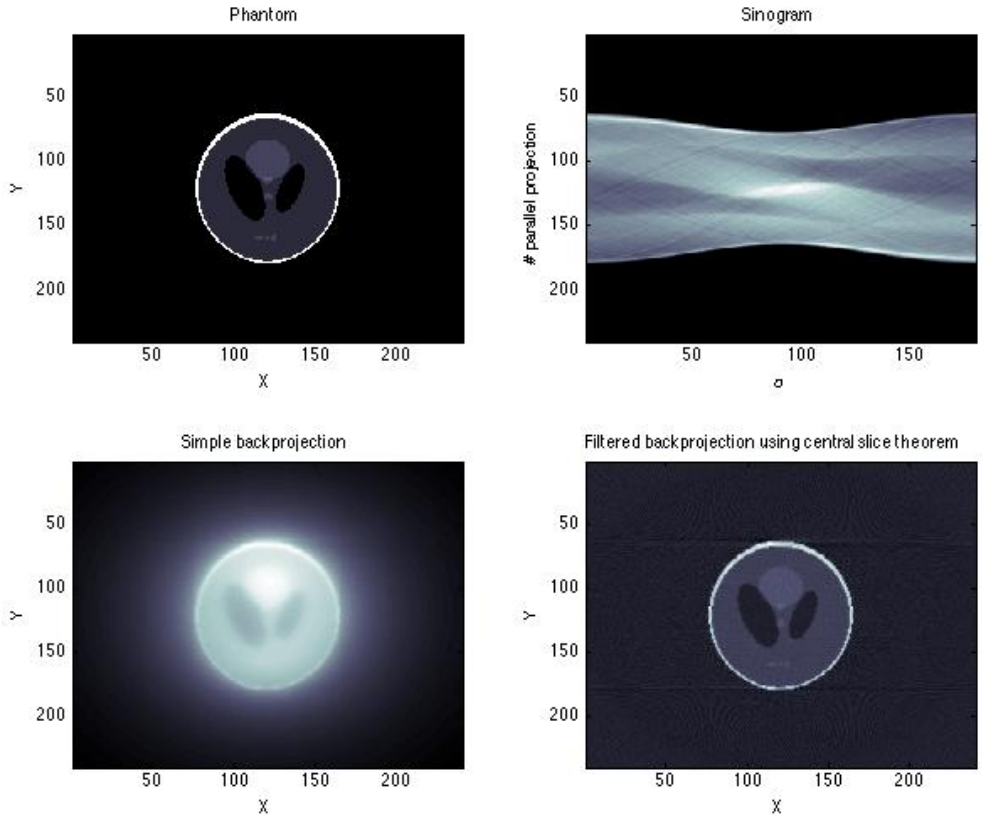

Figure 3.7: The original image, its sinogram and reconstructed (unfiltered and filtered) images of a "Shepp-Logan" phantom

Tomography is often demonstrated on the famous "Shepp-Logan" head phantom. A simple simulation of such was conducted in Matlab.

The results are as shown in Fig. 3.7. The simulation aimed to demonstrate reconstruction approaches used in the experiment and served as a comparison between images underwent unfiltered and filtered back-projection.

As one can see, simple backprojection yielded an image with unnaturally high intensities as a result of the redundancy in the frequency domain. On the other hand, the filtered backprojection (based on Fourier Slice Theorem 2.3.4) returned an image with characteristics more similiar to the original phantom image. The quality of reconstruction was based on the selection of suitable filter and the number of projections. It is noted that there are other filtered backprojection reconstruction approaches: for example, through direct convolution based on Eq. 2.21.

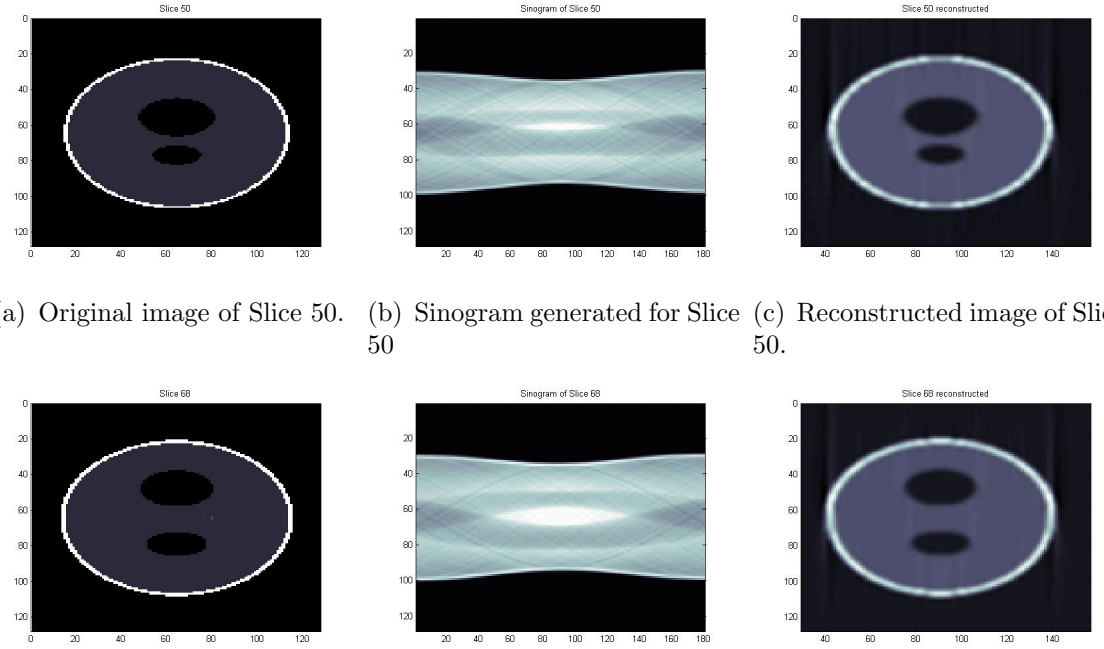

(a) Original image of Slice 50. (b) Sinogram generated for Slice 50 (c) Reconstructed image of Slice 50.

(d) Original image of Slice 68. (e) Sinogram generated for Slice 68 (f) Reconstructed image of Slice 68.

Figure 3.8: Simulation of the reconstruction of 3D object using proposed computing approach.

To illustrate the feasibility of the reconstruction of 3D image from axially stacking 2D reconstructed result, anotehr simulation based on the actual computing procedure was conducted. A 3D array represent-

ing 3D "Shepp-Logan" head phantom was first generated. By radon transformation at angles from zero to 180° at a step of 1°, the resulted 2D projections were then filtered backprojected to generate 181 slices of the phatom. As Fig. 3.2.1 shows, the proposed computing approach worked well.

3.2.2 Computing Approach

The actual reconstruction embraces the principle of filtered back projection using an enhanced version of inverse radon transformation function in Matlab as the kernel. The enhancement was employed by Guizar-Sicairos during his research as published in [Guizar-Sicairos et al., 2011]. The data proccessing include the following steps:

1. Begin by downsizing the file and save as a three dimensional array with the third dimension as angles for further processing.

2. Remove the unwanted linear and constant phase terms generated in the former process of ptychographic reconstruction.

3. Obatin the derivative of the unwrapped data which represents the phase of the image using the algorithm suggested by Guizar-Sicairos in [Guizar-Sicairos et al., 2011].

4. Perform filtered backprojection to obtain the tomogram.

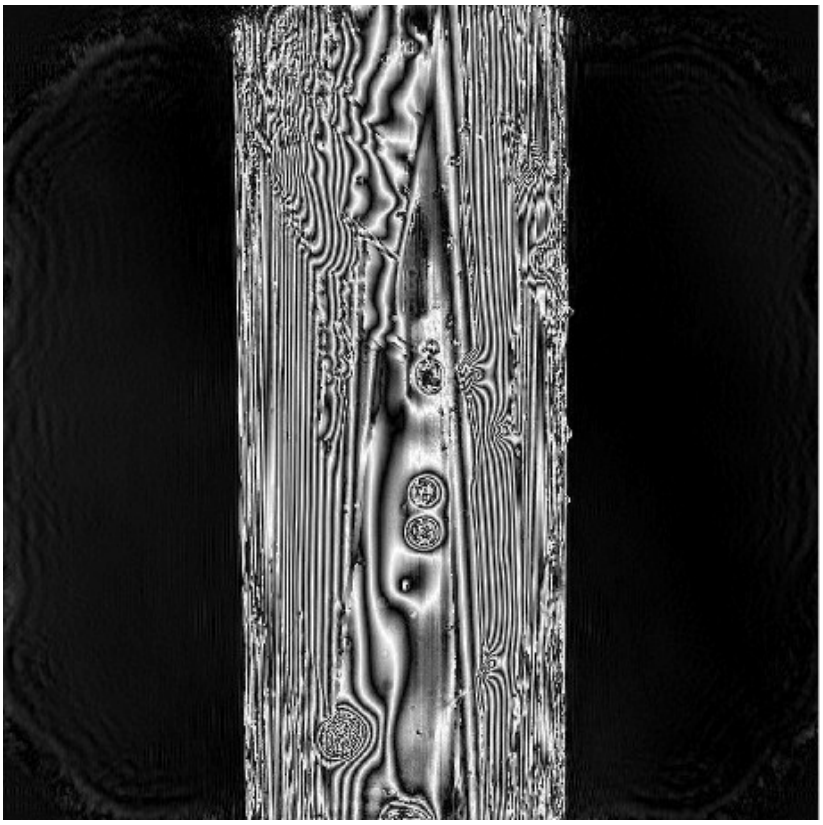

Figure 3.9: Wrapped phase of a projection.

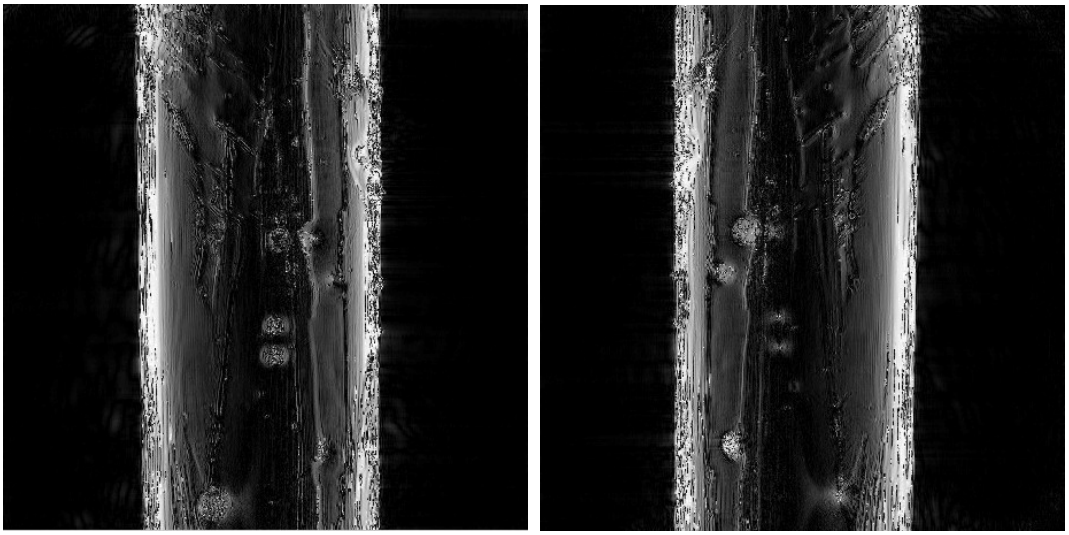

(a) First projection at 0°.

(b) Last projection at 180°.

Figure 3.10: Phase map of projections from computing the derivative of unwrapped regions at two different angles. Fig. 3.10(a) and Fig. 3.9 are of the same area for the same projection.

Given the nature of the differentiation of exponentials, the phase can be generated from unwrapped data fascilitating the fast computation of the tomogram [Guizar-Sicairos et al., 2011] by avoiding the process of unwrapping the phases which was proven a time-consuming procedure. A sample image of the unwrapped phase is shown in Fig. 3.9 and the phase generated through computing the derivatives is given in Fig. 3.10(a). As one can observe, the glass microspheres and residues of the glue on the front and back of the glass tube can be clearly identified in Fig. 3.10(a) and Fig. 3.10(b).

3.2.3 3D Reconstruction

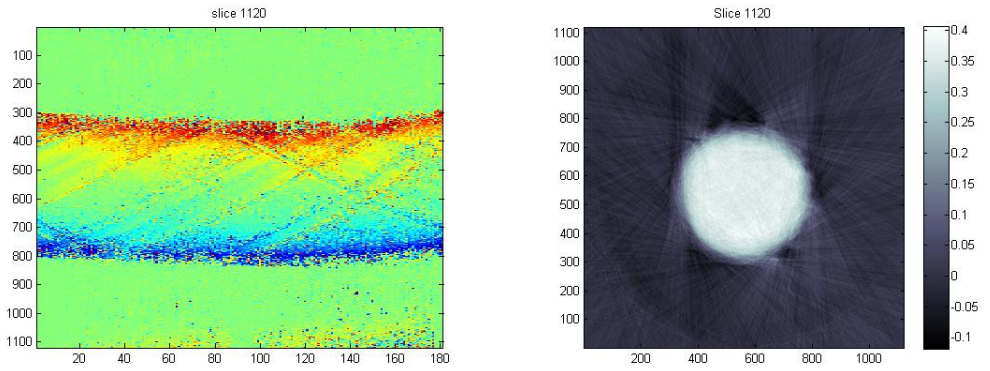

(a) Sample sinogram.

(b) A slice of tomogram reconstructed.

Figure 3.11: Generation of sinograms and filter backprojection of each sinogram to generate its respective slice in the tomogram.

Sinograms were then generated by squeezing each slice of the stacked and phase-corrected 3D data axially along x or y axis of the 2D projections as in Fig. 3.10(a). A sample sinogram looks like Fig. 3.11(a) as shown above. Each sinogram is then fed to the reconstruction ker-

nel to generate slices of the 3D reconstructed object. A sample slice is given in Fig. 3.11(b). As one can see, the slice was as expected a circle with anomalies on the edge of the circle representing the features of the sample, ie, the glass microspheres and the glue.

The central slices from three axis are as shown in Fig. 3.12 below. What was reconstructed in the tomogram is the phase distribution. The phase distribution is related to the whereabout of the material and its refractive indices as phase is the multiplication of refractive index and distance (the depth of the median). As one can see, the tomogram shows the structure of the glass tube revealing the variance of thickness of the tube. The variance of the phase distribution on the tube wall is due to the presence of glass micropheres and transparent glues.

A closer look can verify the direct relationship between phase distribution and structural features. To illustrate, the phase of the first projection at "degree 90" computed from the derivation method is Fig. 3.13, and the central slice cutting this projection in half is give in Fig. 3.14. The three clusters of glass microspheres in Fig. 3.13 were manifested as augments of the pale blue-coloured shapes at the right edge of the glass tube shown in the central slice of Fig. 3.14. The colour scales were opposite in the figures for ease of examing.

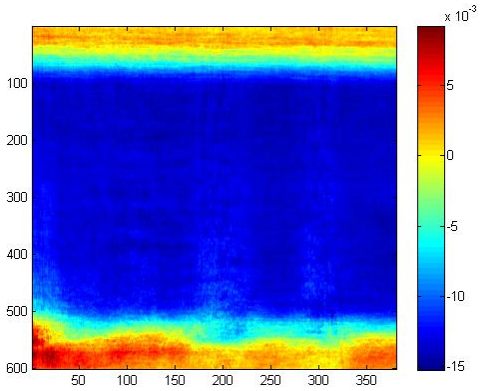

(a) A slice of tomogram along z-axis.

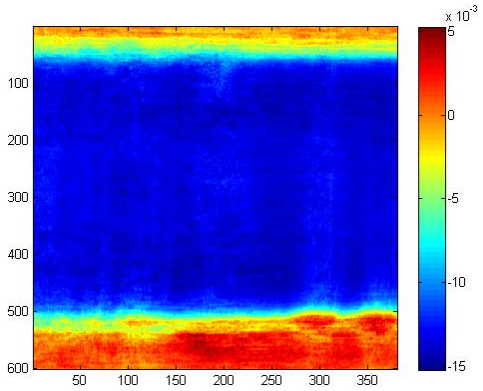

(b) A central slice of tomogram along x-axis

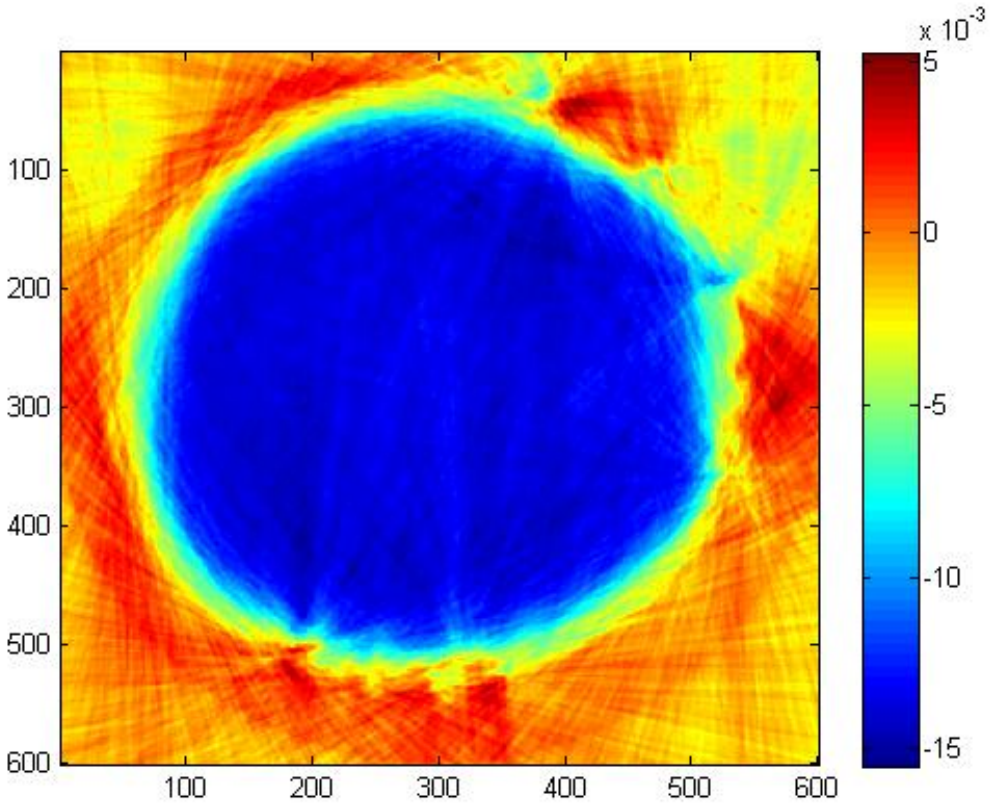

(c) A central slice of tomogram along y-axis

Figure 3.12: Slices of the reconstructed tomogram

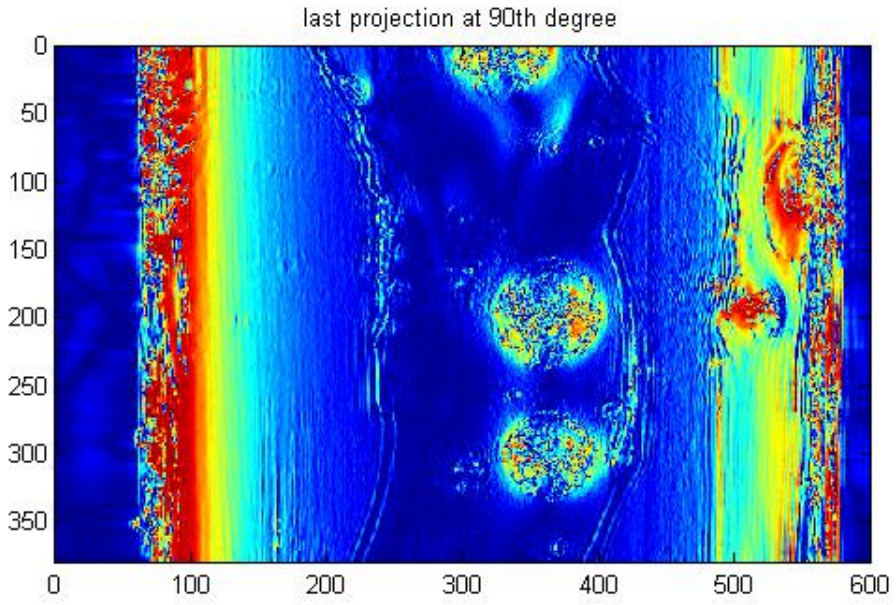

Figure 3.13: Projection at 90 degree.

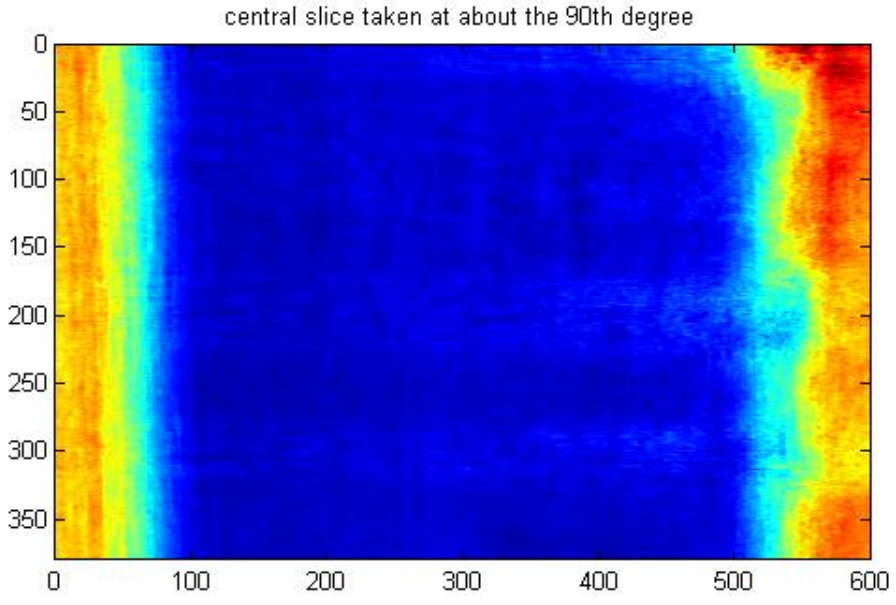

Figure 3.14: Central slice of tomogram cutting at the middle of the projection in Fig. 3.13

It was noted that through the method of computing derivatives suggested by Guizar, the presence of the glue not only increased the phase at its borders (red and yellow regions) but also decreased phase in some areas (deep blue regions around the clusters of microspheres) on Fig. 3.13. That explains the inward augmentation of red region at the upper right corner on Fig. 3.14.

A more conventional approach is to unwrap the phase for each projection using the technique proposed by Goldstein [GOLDSTEIN et al., 1988] before conducting tomographic reconstruction. However, the unwrapping has a much higher requirement for the input data. Not all input projections can have a reasonably low unpaired residue ratio. A comparison of the unwrapping schemes was brought up in the following evaluation part.

3.2.4 Evaluation

Different Unwrapping Schemes

The phase unwrapping scheme proposed by Goldstein [GOLDSTEIN et al., 1988] is a topographic approach to identify, reduce residues, linking positive and negative residues using branch cuts and achieve unwrapping by integration. However, sometime it is difficult to link the corresponding residues. The unpaired residues would become destructive to the sinogram as shown in Fig. 3.15(b). To save time and resources, as well as due to the limited alignment about the rotation axis, the ptychographic reconstructed projections were of limited resolutions and

resonable quality. Thus, not all projections can be unwrapped using the Goldstein method to a quality as high as shown in Fig. 3.15(a). A resulted sinogram such as Fig. 3.15(b) cannot be useful for reconstructing tomogram.

Compared to the Goldstein unwrapping, the derivation method proposed by Guizar [Guizar-Sicairos et al., 2011] is more resilient to unpaired residues. Fig. 3.16(a), the same region as Fig. 3.15(a) only flipped in the y direction shows clearly the features of the sample however the range of values of the phase is much smaller and contains both positive and negative values (refering to the colorbar). As a result, the sinogram formed, as demonstrated in Fig. 3.16(b), has more completed information possible for tomographic reconstruction.

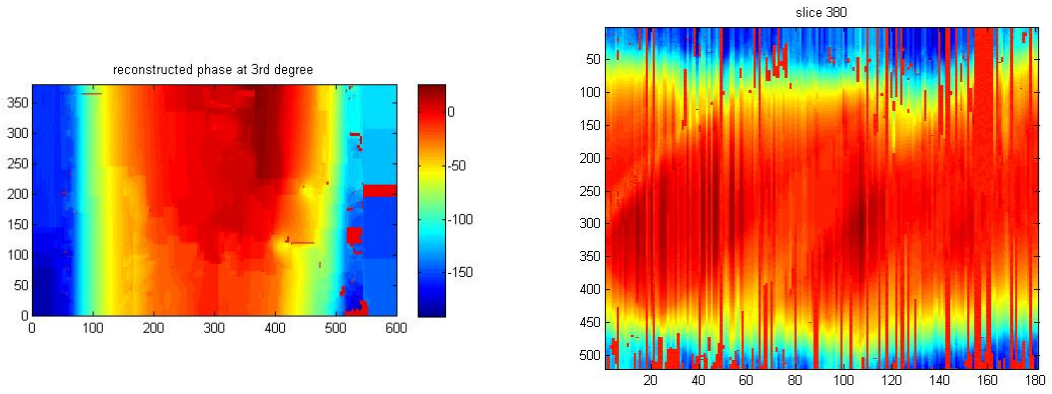

(a) A relatively succesfully unwrapped projection

(b) The not so successful sinogram across all angles.

Figure 3.15: Conventional Goldstein unwrapping

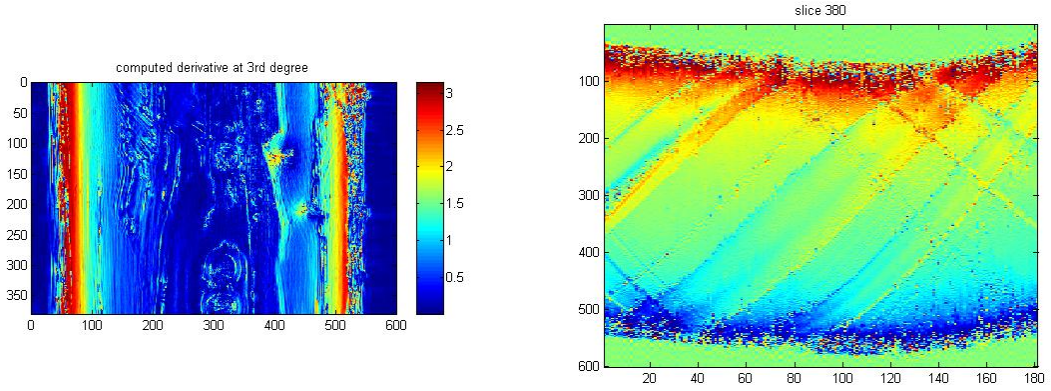

(a) A projection using the derivation method.

(b) A sinogram generated through derivation method that is more successful than Fig. 3.15(b)

Figure 3.16: Computation of derivation

Both sinograms in Fig. 3.15(b) and Fig. 3.16(b) did not lie horizontally as sinograms should. This is due to the misalignment of projections. Hence, the sinogram is a good indicator for the precision of alignments.

Sample Limitations

Tomography can reveal inner features of the object. In this experiment, the optical wave can penetrate the transparent object, however, the absence of inner features deprived of the opportunity to test the aforementioned functionality of tomography.

Technique Limitations

The ptychographic reconstruction algorithm assumes that the sample is 2D. The distance between the sample and the detector is an explicit value for the calculation of the phase distribution of the object

at that specific distance. This inherent characteristic of ptychgraphy contributes to one major systematic error.

The alignment of sample's position with regard to the rotation axis of the motor stage was not ideal as it is done manually. Rotating the sample may vary the distance between the sample and the detector making some of the ptychogrpahic reconstruction out of focus and of subpar quality. Quantitative adjustment could potentially enhance the precision of tomographic reconstruction.

No professional volume rendering program designed for tomographic imaging was used in this experiment. Thus, a more direct viewing of the tomogram cannot be given.

Computation Limitations

The acquisition of data for 181 projections alone is about twelve hours. The reconstruction of each projection took about equal time. It was noted only 100 iterations were run in each reconstruction. More iterations could enhance the quality of the phase map. Increased number of projections at smaller step of angle would also enhance the resolution of tomomgraphic reconstruction. However, the trade-off would be that the experiment would be more time-consuming.

Suggestions for Future Attempts

Some limitations listed above can be overcomed. However, due to limited time given, improvements cannot be made in time for the writting

of this report.

Hence, several measures are suggested here for future attempts:

- A adjuster incorporated on the sample holder that allows better positioning of the sample onto the rotation axis could ensure the quality of the projection reconstructed
- Adopt alignment computation scheme or use fiduciary marker so that the projections could be presicely aligned.
- If enough time was given, iteration number and the number of projections at different angles shall be increased
- Inner features should be included in the sample.
- Professional tomographic imaging softwares such as VGStudio should be used for volume rendering for exracting isosurfaces and direct viewing of the object in 3D.

Chapter 4

Conclusion

In the first part of the report, the physics principles and the technological developments of ptychographic phase retrieval through iterative algorithm was first reviewed followed by a revision of the computerised tomography.

In the second half of the report, the computerised tomography was simulated for a 2D object. By stacking 2D reconstruction together, a 3D tomography simulation was followed to prove the feasibility of the computational approach used in the experiment. In the expriment, the possibility of combining ptychography and tomography using optical waves was explored.

2D phase distribution of the projections of the sample was obtained by computing the derivative of the data in each projection after removing the linear phase terms introduced in the process of ptychographic reconstruction. Using filtered backprojection, the phase density of the sample is retrieved and displayed as a 3D distribution in the tomogram.

As the phase density corresponds to the material density of the sample, the features of the sample, a glass tube glued with glass microspheres on the outer wall, were revealed.

This phase unwrapping approach was briefly compared with the conventional Goldstein phase unwrapping method stating the relative strenghs of each option.

Due to several limitations and the lack of a professional volume rendering software, the resolution of the tomogram was limited, however, the experiment demonstrated that the feasibility of combining the ptychographic phase retrieval and the traditional computerised tomography in optical wave range. Insights on the topic were given as well as the suggestions for future attempts to enhance the performance of this technique.

The tomogram is a phase distribution across the object, which relates to the refractive indices at different parts of the sample as phase is refractive indicies multiplied by distance travelled. This synthesis of imaging techniques is particularly useful in revealing the refractive indices of optical components such as optical fibres. As the fibres are cylindrical, the 3D reconstructed image is a direct map of the refractive indices.

Bibliography

Bauschke, H., Combettes, P., and Luke (2002). Phase retrieval, error reduction algorithm, and Fienup variants: a view from convex optimization. *JOSA A*.

Bean, R. (2012). *Domain Structure Imaging with Bragg Geometry X-ray Ptychography*. PhD thesis.

Born, M. and Wolf, E. (1999). *Principles of Optics*. Cambridge University Press.

Chen, B., Guizar-Sicairos, M., Xiong, G., Shemilt, L., Diaz, A., Nutter, J., Burdet, N., Huo, S., Mancuso, J., Monteith, A., Vergeer, F., Burgess, A., and Robinson, I. (2013). Three-Dimensional Structure Analysis and Percolation Properties of a Barrier Marine Coating. *Scientific Reports*, 3.

Claus, D., Maiden, A., Zhang, F., and Sweeney, F. (2012). Quantitative phase contrast optimised cancerous cell differentiation via ptychography. *Optics*.

Denk, W. and Horstmann, H. (2004). Serial block-face scanning elec-

tron microscopy to reconstruct three-dimensional tissue nanostructure. *PLoS Biology*.

Dierolf, M., Menzel, A., Thibault, P., and Schneider, P. (2010a). Ptychographic x-ray computed tomography at the nanoscale. *Nature*.

Dierolf, M., Thibault, P., Menzel, A., and Kewish, C. (2010b). Ptychographic coherent diffractive imaging of weakly scattering specimens. *New Journal of*, pages 1–15.

Dong, B.-Z., Yang, G.-Z., Gu, B.-Y., and Ersoy, O. K. (1996). Iterative optimization approach for designing an axicon with long focal depth and high transverse resolution. *J. Opt. Soc. Am. A*, 13(1):97–103.

Elser, V. (2003). Phase retrieval by iterated projections. *JOSA A*.

Esmaeili, M., Fløystad, J., Diaz, A., and Høydalsvik, K. (2013). Ptychographic X-ray Tomography of Silk Fiber Hydration. *Marcromolecules*.

Fienup, J. (1978). Reconstruction of an object from the modulus of its Fourier transform. *Optics letters*.

Fienup, J. (1982). Phase retrieval algorithms: a comparison. *Applied optics*.

Fienup, J. (1987). Reconstruction of a complex-valued object from the modulus of its Fourier transform using a support constraint. *JOSA A*.

Fienup, J. and Wackerman, C. (1986). Phase-retrieval stagnation problems and solutions. *JOSA A*.

Gerchberg, R. W. and Saxton, W. O. (1972). A practical algorithm for the determination of the phase from image and diffraction plane pictures. *Optik*, 35:237–246.

GOLDSTEIN, R., ZEBKER, H., and WERNER, C. (1988). Satellite radar interferometry- Two-dimensional phase unwrapping. *Radio Science*.

Guizar-Sicairos, M., Diaz, A., Holler, M., and Lucas, M. (2011). Phase tomography from x-ray coherent diffractive imaging projections. *Optics*.

Guizar-Sicairos, M. and Fienup, J. (2008). Phase retrieval with transverse translation diversity: a nonlinear optimization approach. *Optics express*.

Hegerl, R. and Hoppe, W. (1970). Dynamische Theorie der Kristallstrukturanalyse durch Elektronenbeugung im inhomogenen Primärstrahlwellenfeld. *Berichte der Bunsengesellschaft für physikalische Chemie*, 74(11):1148–1154.

Holler, M., Raabe, J., and Diaz, A. (2012). An instrument for 3D x-ray nano-imaging. *Review of Scientific*.

Hoppe, W. (1982). Trace structure analysis, ptychography, phase tomography. *Ultramicroscopy*.

Huang, B., Wang, W., Bates, M., and Zhuang, X. (2008). Three-dimensional super-resolution imaging by stochastic optical reconstruction microscopy. *Science*.

Jiang, H., Song, C., Chen, C., and Xu, R. (2010). Quantitative 3D imaging of whole, unstained cells by using X-ray diffraction microscopy. In *Proceedings of the*.

Kak, A. C. and Slaney, M. (1988). *Principles of Computerized Tomographic Imaging*. IEEE Press, New York.

Kroupa, M. and Jakubek, J. (2011). High contrast laminography using iterative algorithms. *Journal of Instrumentation*.

Lima, E., Diaz, A., and GUIZARSICAIROS, M. (2012). Cryoscanning xray diffraction microscopy of frozenhydrated yeast. *of Microscopy*.

Maiden, A., Humphry, M., Sarahan, M., and Kraus, B. (2012a). An annealing algorithm to correct positioning errors in ptychography. *Ultramicroscopy*.

Maiden, A., Humphry, M., Zhang, F., and Rodenburg, J. (2011). Superresolution imaging via ptychography. *JOSA A*.

Maiden, A. and Rodenburg, J. (2009). An improved ptychographical phase retrieval algorithm for diffractive imaging. *Ultramicroscopy*.

Maiden, A. M. A., Humphry, M. J. M., and Rodenburg, J. M. J. (2012b). Ptychographic transmission microscopy in three dimensions using a

multi-slice approach. *Journal of the Optical Society of America A*, 29(8):1606–1614.

Marchesini, S. (2007). Invited article: A unified evaluation of iterative projection algorithms for phase retrieval. *Review of Scientific Instruments*.

Miao, J., Charalambous, P., Kirz, J., and Sayre, D. (1999). Extending the methodology of X-ray crystallography to allow imaging of micrometre-sized non-crystalline specimens. *Nature*.

Nellist, P., McCallum, B., and Rodenburg, J. (1995). Resolution beyond the'information limit'in transmission electron microscopy. *1995*.

Penczek, P. (2010). Fundamentals of three-dimensional reconstruction from projections. *Methods in enzymology*.

Rodenburg, J. (2008). Ptychography and related diffractive imaging methods. *Advances in Imaging and Electron Physics*.

Rodenburg, J. and Faulkner, H. (2004). A phase retrieval algorithm for shifting illumination. *Applied Physics Letters*.

Rodenburg, J. M. and Bates, R. H. T. (1992). The Theory of Super-Resolution Electron Microscopy Via Wigner-Distribution Deconvolution. *Philosophical Transactions of the Royal Society A: Mathematical, Physical and Engineering Sciences*, 339(1655):521–553.

Sayre, D. (1952). Some implications of a theorem due to Shannon. *Acta Crystallographica*, 5(6):843–843.

Schermelleh, L., Heintzmann, R., and Leonhardt, H. (2010). A guide to super-resolution fluorescence microscopy. *The Journal of Cell Biology*, 190(2):165–175.

Seiler, M. C. and Seiler, F. A. (1989). *Numerical Recipes in C: The Art of Scientific Computing*, volume 9.

Shannon, C. (1949). Communication in the presence of noise. In *Proceedings of the IRE*.

Thibault, P., Dierolf, M., Menzel, A., Bunk, O., and David, C. (2008). High-resolution scanning x-ray diffraction microscopy. *Science*.

Trtik, P., Diaz, A., Guizar-Sicairos, M., and Menzel, A. (2012). Density mapping of hardened cement paste using ptychographic X-ray computed tomography. *Cement and Concrete*.

Vine, D., Williams, G., Nugent, K., Abbey, B., and Pfeifer, M. (2009). Ptychographic Fresnel coherent diffractive imaging. *Physical Review A*, pages 1–5.

Xu, F., Helfen, L., Baumbach, T., and Suhonen, H. (2012). Comparison of image quality in computed laminography and tomography. *Optics express*.

Yang, C., Qian, J., Schirotzek, A., Maia, F., and Marchesini, S. (2011). Iterative Algorithms for Ptychographic Phase Retrieval.

Zhuang, X. (2009). Nano-imaging with STORM. *Nature Photonics*.

Appendix A

List of Main Equipments

- Thermo Scientific Duke Standards^{TM}dry soda lime glass microspheres, Part NO.9030.
- Three Newport^{TM}translation stage, Model MFA-CC.
- One Newport^{TM}rotation stage, Model SR50CC
- One Thorlabs^{TM}Molded Glass Aspheric Lens, Model A375-A
- Laser of wavelength of 543.5nm
- One Neo sCMOS from Andor^{TM}
- One pinhole of the size about 800nm
- One stage holder CADed by the author
- One sample holder CADed by the authro